Semidilute Athermal Polymer Solutions near a Hard Wall

Wan Y. Shih,* Wei-Heng Shih, and Ilhan A. Aksay

Department of Materials Science and Engineering, and Advanced Materials Technology Center, Washington Technology Centers, University of Washington, Seattle, Washington 98195

Received August 18, 1989; Revised Manuscript Received January 26, 1990

ABSTRACT: We have studied semidilute athermal polymer solutions near a hard wall extensively with Monte Carlo simulations. The details of the segment density profiles near the wall are shown for the first time. We have shown that in the semidilute regime the segment density near a wall has the form: $\phi(z) = \phi(1 - e^{-(z/\xi)^m})$, where m is the exponent at small distance and ϕ and ξ are the bulk segment density and the bulk correlation length, respectively. This form fits remarkably well with the Monte Carlo simulations and was derived using an argument similar to Weibull's for the failure of materials. We show m to be $\sim$1.6 in agreement with de Gennes' scaling prediction. The first-layer segment density, ϕ_1, from the simulations behaves as $\phi_1 \sim \phi^{2.2}$, similar to the bulk osmotic pressure. The radius of gyration, R_G, and the deduced correlation length, ξ, are also in accordance with the scaling predictions and the experiments.

I. Introduction

A semidilute polymer solution is one in which polymers overlap. The bulk properties of semidilute polymer solutions have been studied extensively,[1-3] and much is known. The scaling theory, especially, has been very successful.[1,2] The predictions of the scaling theory about various physical quantities as a function of polymer concentration, c, have been confirmed experimentally.[1,3] For example, in the case of a good solvent, the correlation length, ξ, behaves as $\xi \sim c^{-3/4}$; the radius of gyration, R_G, behaves as $R_G^2/N \sim c^{-1/4}$, where N is the degree of polymerization; and the osmotic pressure, Π, behaves as $\Pi \sim c^{9/4}$. The scaling $R_G^2/N \sim c^{-1/4}$ has also been observed in Monte Carlo simulations.[4]

Although the bulk properties of semidilute polymer solutions have been studied well, the interfacial properties of a semidilute polymer solution are less well-known. For example, the density profiles near a hard wall are difficult to examine experimentally. When a polymer solution is near a hard wall, it is thought that the polymer concentration is depleted in the proximity of the wall and the thickness of the depleted layer is on the order of the correlation length, ξ. For semidilute polymer solutions in a good solvent, de Gennes predicts that the polymer concentration rises in a power law fashion as $c(z) \sim (z/\xi)^m$, where z is the distance away from the wall and $m = {}^5/_3$.[2,5] By arguing that the bulk osmotic pressure, Π, should be proportional to the first-layer concentration $c(z=1)$, de Gennes[2] predicts that, in a lattice model, the concentration in the first layer near the wall behaves as $c(z=1) \sim c^{9/4}$. Though interfacial properties are technologically important, detailed study of polymer solutions near a wall, especially the determination of the concentration profiles, is experimentally difficult. Polymers near or at a surface or polymers between two walls have been a topic of extensive Monte Carlo simulations[6-10] and mean-field calculations.[11,12] References 6 and 7 dealt with the adsorption of polymers in a dilute solution near an attractive wall. Reference 8 studied two-dimensional concentrated polymer solutions between two walls and compared the osmotic pressure to the first-layer segment density near the wall. References 9 and 10 studied polymer melts between two planes. References 11 and 12 studied the adsorption of polymers and the interaction between two walls with adsorbed polymers. Mean-field calculations may work well for more concentrated polymer solutions or polymer solutions near the Θ temperature. For dilute and semidilute athermal polymer solutions, Monte Carlo simulations are more representative since the scaling $R_G^2/N \sim c^{-1/4}$ has indeed been found.[4] The purpose of the present paper is therefore to use the Monte Carlo simulations to study semidilute polymer solutions near a hard wall and to give a detailed account for the density profiles. Because of the availability of the force balance measurements between two colloidal surfaces, it is important to have a detailed knowledge of the segment density profiles near a wall in order to understand the forces between two walls. The detailed knowledge of the segment density profiles near a wall is essential in understanding the forces between two surfaces. We find that the segment density profiles near a hard wall can be fitted remarkably well to the form of $1 - e^{-(z/\xi)^m}$ for which we have provided a derivation using an argument similar to Weibull's[13] probability of failure in materials. The value of the resultant exponent m agrees with the scaling prediction of de Gennes.[2,4] The parameter ξ turns out to be the bulk correlation length, and the scaling of ξ with segment density is in good agreement with the experiment of Daoud et al.[1] Our results suggest that $1 - e^{-f(z)}$ should be a general form for monotonically varying density profiles near an interface where $f(z)$ is a function of z, bearing the details of the spatial density correlation, which may differ from system to system. In the present case, $f(z) = (z/\xi)^m$.

In the remainder of this paper, section II describes the model. Section III contains the results. Section IV gives the derivation for the segment density profiles, and section V, the conclusion.

II. Model

We consider an $N_x \times N_y \times N_z$ cubic lattice as illustrated in Figure 1, in which there are M polymer chains each with N segments, represented by the full circles in Figure 1. For polymers in an athermal solution, we assume there is no interaction between the segments except volume exclusion, which is taken into account by allowing no more than one segment to occupy one lattice site. There are two hard walls on the top at $z = 0$ and at the bottom at $z = N_z + 1$, as shown in Figure 1. By hard wall we mean the wall is impenetrable for the polymers. In the x and y directions, we use periodic boundary conditions.

Polymers of N segments are generated (polymerized) as follows.[14] We first randomly choose an unoccupied

0024-9297/90/2223-3291$02.50/0

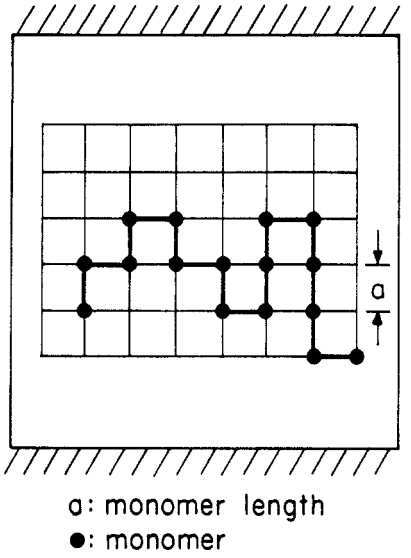

Figure 1. Schematic of the model. Hard walls are on the top and at the bottom of the Monte Carlo cell. The full circles denote the segments.

site to locate the first segment of a chain. Once the ith segment is located, the $i + 1$th segment is then placed at random at one of the unoccupied neighboring sites of the ith segment. If all the neighboring sites of the ith segment have already been occupied and $i < N$, the partial configuration is then discarded and a new chain is generated. Using this procedure, one can generate chains of a fixed number (N) of segments. Polymerization continues until the desired number of chains is reached.

Once the polymerization is done, the chains begin to move. Three types of movement are considered in the simulation. The first type of motion is the Brownian motion, namely, the polymer chains move as a whole in a random fashion as illustrated in Figure 2a. The second type of motion is polymer wiggle; specifically, a segment in a chain flips,[15] as illustrated in Figure 2b. The third type of motion is reptation; that is, either end of a chain moves randomly to an adjacent unoccupied site and drags the rest of the chain along a *tube* that is shaped by its body[16] as illustrated in Figure 2c. Reptation is especially important when the density is high because the first two types of motions cannot effectively move the polymers. The motion of a polymer chain may be hindered by the presence of other polymers and/or by itself (that is, the motion of one part of a polymer chain can be hindered by another part of the chain). In general, each type of motion may be associated with a different time constant. Thus, in the simulation, each type of motion should be attempted with a different frequency. However, for convenience, we choose the same attempt frequency for all movements. That is, in each Monte Carlo step, the Brownian motion and the reptation of each chain and the flipping of each segment are attempted once.

In all the simulations, for a given N, we choose N_x, N_y, and N_z such that they are all at least 8 times larger than the radius of gyration, R_G, to ensure that the obtained R_G is not affected by the boundary conditions of the Monte Carlo cell. In each run, we discard 2000–6000 Monte Carlo steps since the initial configurations are generated at random and are not the equilibrium configurations. The results are the average over 5000–10000 Monte Carlo steps. For a given initial concentration $\phi_{av} = MN/N_xN_yN_z$, we perform 2–4 independent runs.

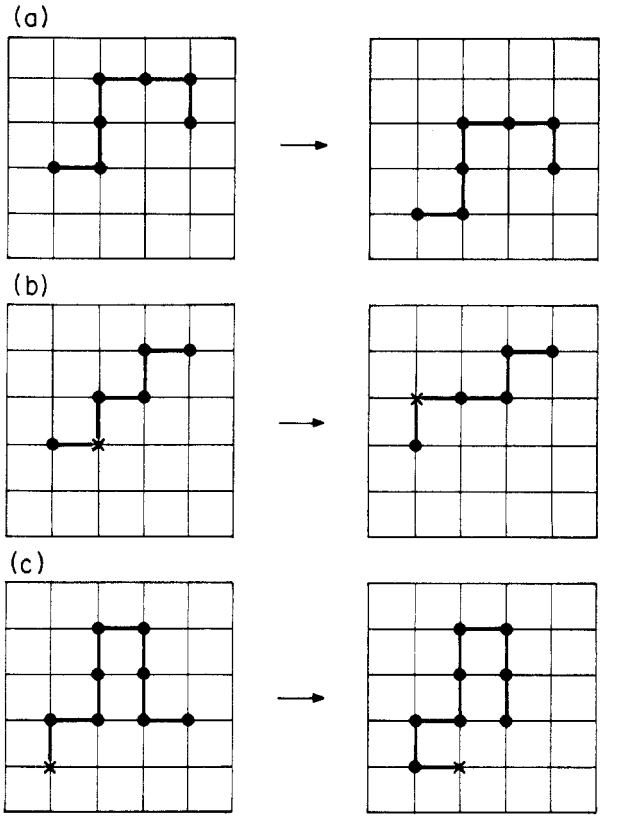

Figure 2. (a) Brownian motion of the chain, (b) flipping of a segment within a chain, and (c) reptation of a chain.

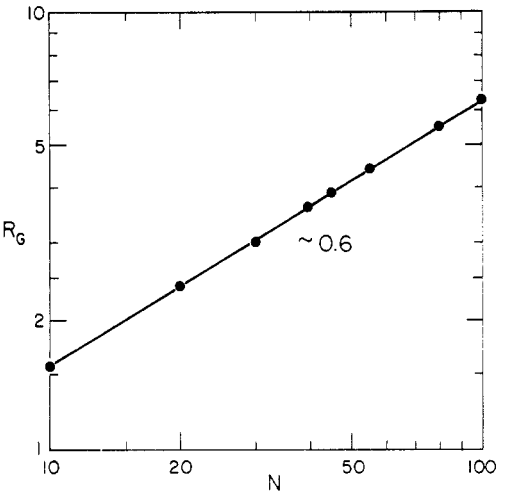

Figure 3. R_G vs N for dilute solutions, where R_G is the radius of the gyration and N is the degree of polymerization.

III. Results

An athermal solution corresponds to the case that the χ parameter in the Flory–Huggins language is zero. We first show in Figure 3 the double-logarithmic plot of the radius of gyration, R_G, of polymers with degree of polymerization N versus N in the dilute regime where R_G is defined as

$$R_G^2 = \frac{1}{2N^2}\sum_{i=1}^{N}\sum_{j>i}|\vec{r}_i - \vec{r}_j|^2 \qquad (1)$$

in which $\vec{r}_i$ is the position of the ith segment of a chain. The slope in Figure 3 is 0.6, which agrees with Flory's number ν, which is 0.6 for athermal polymer solutions[17] and is also within the numerical error of the self-avoiding random walks,[17] which is 0.59.

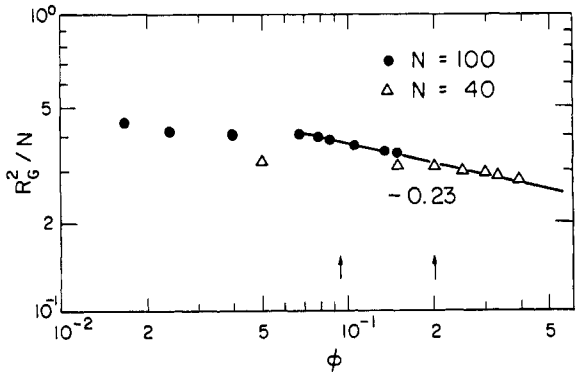

Figure 4. R_G^2/N vs ϕ for $N = 40$ (△) and for $N = 100$ (●) where R_G and N are as defined in Figure 3 and ϕ is the bulk segment density.

One may define the segment density, ϕ, as the average occupancy of a lattice site by a segment. The segment density, ϕ, is related to the weight concentration, c, as $c = m\phi/a^3$ where m is the molecular weight of a segment and a is the segment length (lattice constant in the model). Throughout this text, we will use ϕ rather than c for convenience. Notice that the segment we refer to in the model may be different from an actual repeating unit in a polymer, which is normally fat and short and unable to bend with a large angle. While the segment in the model is capable of making 90° bends, one may think of the segment in the model as a group of successive repeating units in a real polymer. Thus, the chains with N segments in the model may correspond to real polymers whose degree of polymerization is several times larger than N.

As one increases the segment density, at some point one passes from the dilute regime, where chains are well separated, to the semidilute regime, where chains overlap. An estimate of the crossover segment density, ϕ^*, from the dilute solution to the semidilute solution may be made by

$$\phi^* = N/(4\pi/3)R_G^3 \tag{2}$$

where N is the number of segments in a chain or the degree of polymerization and R_G is the radii of gyration of the chains, respectively. One can calculate ϕ^* readily from Figure 3. For example, when $N = 40$, $R_G = 3.6$, and therefore, $\phi^* = 0.2$; when $N = 100$, $R_G = 6.3$, and $\phi^* = 0.095$.

***R*$_G$ vs ϕ.** Because of the overlapping of chains, a semidilute solution is very different from a dilute solution. For instance, for a given N, the radius of gyration, R_G, is independent of the segment density in dilute solutions but has ϕ dependence in the semidilute regime:[1,4] $R_G^2/N \sim \phi^{-1/4}$. We show R_G^2/N versus the segment density, ϕ, in a double-logarithmic plot in Figure 4 where full circles represent $N = 100$ and triangles represent $N = 40$. In both cases, R_G remains constant at low segment densities. At higher segment densities the two sets of data fall on one line with a slope −0.23, which is within the numerical error bars of the value $-1/4$ predicted by the scaling theory. It should be mentioned here that the exponent −0.23 was determined solely from the data points without fitting it to any functional form, which is different from ref 4 where a similar scaling is obtained by comparing a line of a given slope to a few data points. The conventional wisdom is that one must have long polymers (large N) in order to have a wider semidilute density region for the scaling analysis. However, in the present paper, we show that we were able to capture the scaling of R_G^2/N accurately without using a large value of N by combining two sets of data of relatively small N ($N = 40$ and 100) to obtain a fairly wide density range for the scaling analysis as shown in Figure 4. This is made possible by the fact that various physical quantities such as R_G^2/N, the correlation length ξ, and the osmotic pressure Π depend solely on the segment density ϕ and do not depend on N in the semidilute regime. Therefore, data points of different values of N fall on one curve in the semidilute regime as we have shown in Figure 4. Thus, the combination of two sets of data of small N still allows the accurate determination of the scaling behavior. Notice that R_G changes from dilute-solution behavior to semidilute-solution behavior at about the estimated crossover segment density, ϕ^*, which is 0.095 for $N = 100$ and 0.2 for $N = 40$, as indicated by arrows in Figure 4. In the following, we will focus on the density profiles near a wall in the semidilute regime where R_G^2/N shows the ϕ dependence.

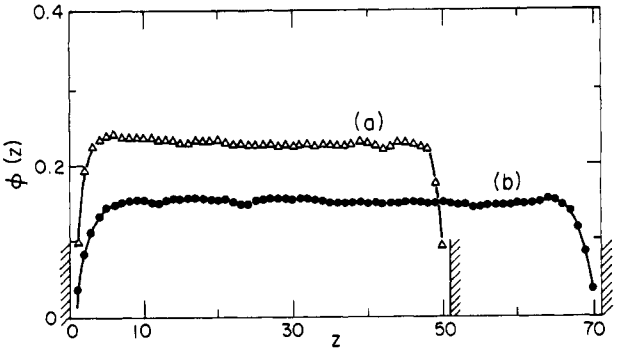

Figure 5. Typical segment density profiles from $z = 1$ to N_z for (a) $N = 40$ with the bulk segment density $\phi \sim 0.23$ and (b) $N = 100$ with the bulk segment density $\phi \sim 0.15$. Notice that for profile (a) the walls are at $z = 0$ and $z = 51$ and for profile (b) the walls are at $z = 0$ and $z = 71$.

Density Profiles. Typical density profiles in the semidilute regime are shown in Figure 5. Curve (a) is for $N = 40$ in a $35 \times 35 \times 50$ lattice with the bulk segment density $\phi \sim 0.23$, and curve (b) is for $N = 100$ in a $50 \times 50 \times 70$ lattice with the bulk segment density $\phi \sim 0.15$. The segment density is indeed smaller near the walls and rises monotonically toward the bulk value. The thickness of the depletion layer is on the order of the correlation length, as evidenced by the wider depletion layers in curve (b) where the correlation length, ξ, is larger than that in curve (a), as described in more detail below. A closer look at the density profiles near the wall shows density profiles $\phi(z)$ versus z in a double-logarithmic plot for $N = 100$ in Figure 6, where z is the distance away from the wall and $\phi(z)$ is the segment density at distance z. The extrapolated slope at small z is (a) 1.23 for $\phi = 1.35$, (b) 1.27 for $\phi = 0.107$, and (c) 1.41 for $\phi = 0.0925$, where ϕ is the bulk density. The extrapolated slope decreases with increasing bulk segment density and does not agree with the value $5/3$ predicted by the scaling theory. The reason for the disagreement is that even with $N = 100$ the correlation length is still not large enough. In order to have the correct extrapolated slope at small z, one should have $z/\xi \ll 1$. Therefore, instead of extrapolating the exponent directly from the segment density profiles at small z, we use the following scaling form for the segment density profiles

$$\phi(z) = \phi(1 - e^{-(z/\xi)^m}) \tag{3}$$

where ϕ is the bulk segment density and ξ is the correlation length. The physical meaning of this profile will be discussed later. This scaling function gives the right behavior both at small z and at large z. At small z/ξ,

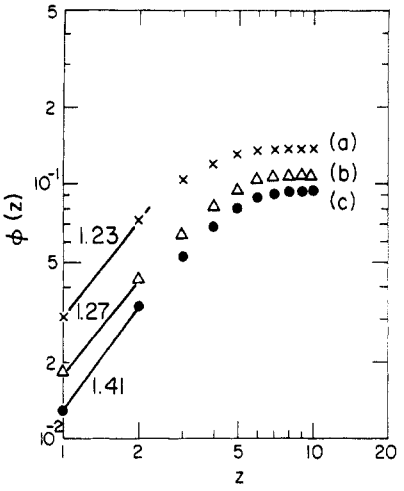

Figure 6. Close-up of the segment density profiles for N = 100 near the wall (a) ϕ = 0.135, (b) ϕ = 0.107, and (c) ϕ = 0.0925, where ϕ is the bulk segment density.

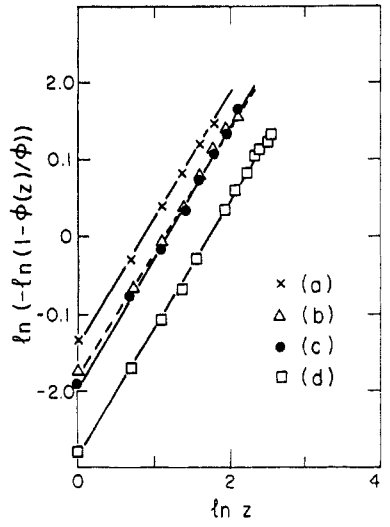

Figure 7. ln {-ln [1 - $\phi(z)/\phi$]} vs ln z. The fitted values for the exponent m and the correlation length ξ are (a) m = 1.64 and ξ = 2.3 for ϕ = 0.135, (b) m = 1.61 and ξ = 2.8 for ϕ = 0.107, (c) m = 1.68 and ξ = 3.2 for ϕ = 0.0925, and (d) m = 1.63 and ξ = 5.9 for ϕ = 0.0167.

$\phi(z)$ increases in a power law fashion with z: $\phi(z) \sim (z/\xi)^m$. At $z/\xi \gg 1$, $\phi(z)$ gives the bulk density ϕ. We fit the three density profiles shown in Figure 6 to the above form, and the results are shown in Figure 7. One can see that the fit is extremely good. From the lines in Figure 7, we extract the exponent m, which is the slope of the lines, and the correlation length, ξ, which is $e^{y_0/m}$, where $-y_0$ is the intercept of the lines with the y axis: (a) m = 1.64 and ξ = 2.3 for ϕ = 0.135; (b) m = 1.61 and ξ = 2.8 for ϕ = 0.107; and (c) m = 1.68 and ξ = 3.2 for ϕ = 0.0925. The extracted values of both m and ξ are very reasonable: (1) the values for m are in very good agreement with the value $^5/_3$ predicted by the scaling theory and (2) the values for ξ show the right trend for decrease with increasing bulk concentration.

Exponent m. Throughout the whole semidilute density range that we have simulated (up to ϕ = 0.16 for N = 100 and ϕ = 0.32 for N = 40), the scaling function, eq 3, fits the segment density profiles remarkably well. For the exponent m, we always obtain values around 1.6 (ranging from 1.55 to 1.7), in good agreement with the scaling theory of de Gennes. We have also studied the segment density profiles in the dilute regime. Although the segment density profiles are more complicated in the dilute regime, we also get a very good fit if we use only the portion of the density profiles that are near the wall. An example is shown in curve (d) in Figure 7, where we obtain m = 1.63 and ξ = 5.9. Thus, the segment density near the wall is proportional to $(z/\xi)^{5/3}$ in both dilute and semidilute solutions, except that $\phi(z)$ increases monotonically in semidilute solutions but undergoes a maximum before reaching the bulk density value in dilute solutions. A more detailed account of the density profiles in the dilute regime will be published in a separate paper.

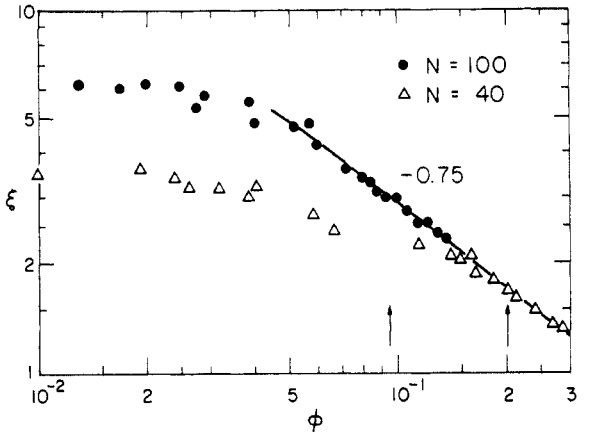

Figure 8. ξ vs ϕ for N = 40 (△) and for N = 100 (●) where ξ is the correlation length and ϕ is the bulk segment density. Arrows indicate ϕ^*.

Correlation Length ξ. We show the extracted values of ξ versus the bulk segment density, ϕ, in a double-logarithmic plot in Figure 8 where full circles and triangles represent N = 100 and N = 40, respectively. (1) ξ is independent of the segment density at low segment densities. Notice that the values of ξ at low segment densities are approximately equal to the values of the radii of gyration, $R_G \sim$ 6.3 for N = 100 and ~3.6 for N = 40, which is in agreement with the notion that in the dilute regime the polymers are well separated and the correlation length is equal to the radius of gyration of the chains. (2) When the segment density reaches the crossover density, ϕ^*, the two sets of data fall on one line with a slope ~-0.75, in agreement with the scaling prediction that the correlation length, ξ, in the semidilute regime depends only on the segment density and behaves as $\xi \sim \phi^{-3/4}$. The estimated values of ϕ^* for N = 100 and for N = 40 are indicated by arrows in Figure 8. Again, the accurate determination of the exponent of ξ with relatively small values of N is made possible by the combination of two sets of data of different values of N that fall on the same curve in the semidilute regime where the correlation length, ξ, depends only on ϕ and does not depend on N, as we have argued above. The effect of N is to change the value of the crossover segment density, ϕ^*. In view of the remarkable result for the correlation length, ξ, obtained from the segment density profiles near a wall, this may turn out to be an easier way of calculating the correlation length. Normally, the correlation length is obtained from calculating the density–density correlation function, which is very time-consuming in Monte Carlo simulations.

ϕ_1 vs ϕ. In Figure 9, we plot ϕ_1 versus ϕ where ϕ_1 is the segment density at z = 1 and ϕ is the bulk segment density, as represented by the plateau in Figures 5 and 6, for the semidilute regime. Full circles represent N = 100, and triangles represent N = 40. Again, the estimated crossover segment density, ϕ^* = 0.095 for N = 100 and ϕ^* = 0.2 for N = 40, are indicated by arrows. One can see that, above the crossover segment densities,

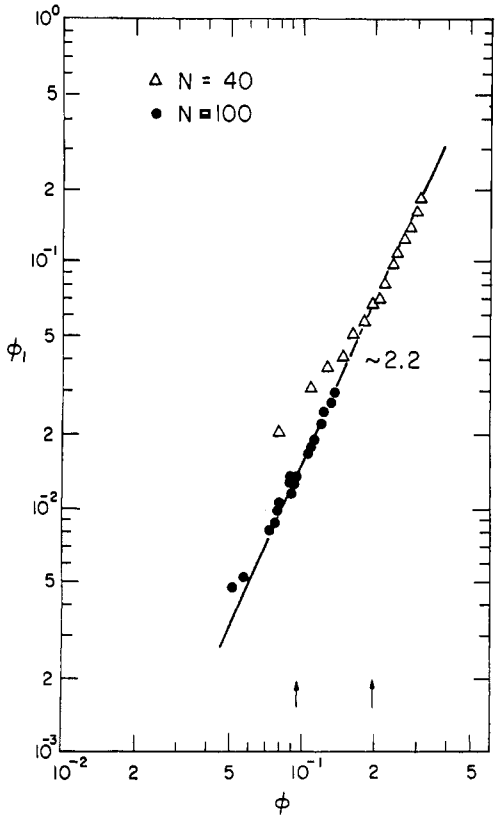

Figure 9. ϕ_1 vs ϕ for $N = 40$ (△) and for $N = 100$ (●) where ϕ_1 is the first-layer segment density near the wall and ϕ is the bulk segment density.

the two sets of data fall on one line with a slope ~2.2, indicating that the behavior of the first-layer segment density is indeed similar to that of the bulk osmotic pressure, Π, which behaves as $\Pi \sim \phi^{9/4}$. As with R_G^2/N and ξ, the accurate determination of the exponent of ϕ_1 is due to the combination of two sets of data of different values of N, which fall on the same curve in the semidilute regime, where ϕ_1 depends only on ϕ and does not depend on N.

IV. Discussion

We have shown that the segment density profiles of polymer solutions near a hard wall can be fitted to the form of eq 3 very well. The resultant exponent m is in agreement with the scaling prediction of de Gennes.[2,5] The parameter ξ turns out to be the bulk density–density correlation length and is in excellent agreement with the experiment of Daoud et al.[1] This suggests that eq 3 is not merely a fitting functional form but has some deeper physical meaning. Below, we present an argument similar to Weibull's for the probability of failure in materials.[13]

Since $\phi(z)$ is the segment density at z, $P(z) \equiv \phi(z)/\phi$ can be viewed as the relative probability of finding a segment at position z to that of finding a segment in the bulk. Given n segments, the relative probability of finding one of the n segments at position z is $P_n(z)$. The relative probability that none of the n segments are at position z is thus $1 - P_n(z)$, which is expected to be

$$1 - P_n(z) = (1 - P(z))^n \tag{4}$$

Since $P(z)$ and $P_n(z)$ should have the same functional form, we have

$$P(z) \equiv \frac{\phi(z)}{\phi} = 1 - e^{-f(z)} \tag{5}$$

and

$$P_n(z) = 1 - e^{-nf(z)} \tag{6}$$

where $f(z)$ is a function of z. The negative sign in the exponents of eqs 5 and 6 is used to ensure that both $P(z)$ and $P_n(z)$ are finite when $f(z)$ is such that

$$f(z) \to 0 \text{ as } z \to 0 \text{ since } P(0) = 0 \tag{7}$$

and

$$f(z) \to \infty \text{ as } z \to \infty \text{ since } P(\infty) = 1 \tag{8}$$

To satisfy eqs 7 and 8, $f(z)$ can be any increasing function of z. The form of $f(z)$ may vary from system to system depending on the detail of the spatial density–density correlation. In the present case, we choose $f(z)$ to be $(z/\xi)^m$ to take into account the power law segment–segment correlation in a polymer solution. We believe that the form of eq 5 is a general one for monotonically varying density profiles. In many systems, the interfacial density profiles are known to decay exponentially into the bulk except that the form of $f(z)$ may be different for different systems.

V. Conclusion

In summary, we have studied semidilute polymer solutions near a hard wall extensively. In the Monte Carlo simulations, the semidilute regime was identified using the ϕ dependence of the radius of gyration: $R_G^2/N \sim \phi^{-0.23}$. In the semidilute regime, the segment density is depleted near the wall, and the thickness of the depletion layer is on the order of the correlation length. We have determined the segment density profile near a hard wall to have the form: $\phi(z) = \phi(1 - e^{-(z/\xi)^m})$ [eq 3]. This form fits remarkably well with the Monte Carlo simulations and was derived using an argument similar to Weibull's for the failure of materials. We found (1) the value of m to be from 1.55 to 1.7 and (2) ξ to be the bulk correlation length in that ξ equals R_G and remains constant in the dilute regime and behaves as $\xi \sim \phi^{-0.75}$ in the semidilute regime, which is in agreement with the experiment and also with the scaling theory. For $z/\xi \ll 1$, our profile [eq 3] agrees with de Gennes'[1] scaling prediction: $\phi(z) \sim (z/\xi)^m$ with $m \cong 5/3$.

The first-layer segment density near a wall, ϕ_1, was shown from the simulations to behave as $\phi_1 \sim \phi^{2.2}$, which indicates that the ϕ dependence of ϕ_1 in the semidilute regime is the same as that of the osmotic pressure, which is known to behave as $\Pi \sim \phi^{9/4}$.

Acknowledgment. This work was supported by the Air Force Office of Scientific Research (AFOSR) and the Defense Advanced Research Projects Agency (DARPA) under Grant No. AFOSR-87-0114.

References and Notes

(1) Daoud, M.; Cotton, J. P.; Farnoux, B.; Jannink, G.; Sarma, G.; Benoit, H.; Duplessix, R.; Picot, C.; de Gennes, P.-G. *Macromolecules* **1975**, *8*, 804.
(2) de Gennes, P.-G. *Scaling Concepts in Polymer Physics*; Cornell University Press: Ithaca, NY, 1979; Chapter III and references cited therein.
(3) Okano, K.; Wada, E.; Taru, Y.; Hiramatsu, H. *Rep. Prog. Polym. Sci. Jpn.* **1974**, *17*, 141.
(4) Bishop, M.; Kalos, M. H.; Sokal, A. D. *J. Chem. Phys.* **1983**, *79*, 3496.
(5) de Gennes, P.-G. *Macromolecules* **1981**, *14*, 1637.
(6) Eisenriegler, E.; Kremer, K.; Binder, K. *J. Chem. Phys.* **1982**, *77*, 6296.
(7) Kremer, K. *J. Chem. Phys.* **1985**, *83*, 5882.
(8) Dickman, R.; Hall, C. K. *J. Chem. Phys.* **1982**, *77*, 6296.

(9) ten Brinke, G.; Ausserre, D.; Hadziioannou, G. *J. Chem. Phys.* **1988**, *89*, 4374.
(10) Kumar, S. K.; Vacatello, M.; Yoon, D. Y. *J. Chem. Phys.* **1988**, *89*, 5206.
(11) Scheutjens, J. M. H. M.; Fleer, G. J. *J. Phys. Chem.* **1979**, *83*, 1619.
(12) Scheutjens, J. M. H. M.; Fleer, G. J. *Macromolecules* **1985**, *18*, 1882.
(13) Weibull, W. J. *Appl. Mech.* **1951**, *18*, 293.
(14) Rosenbluth, M. N.; Rosenbluth, A. W. *J. Chem. Phys.* **1955**, *23*, 356.
(15) Verdier, P. H.; Stockmayer, W. H. *J. Chem. Phys.* **1962**, *36*, 227.
(16) Wall, F. T.; Mandel, F. *J. Chem. Phys.* **1975**, *63*, 4592.
(17) For a review, see ref 2 and the references therein.

Stiffness of Oriented Flexible-Chain Polymers

Aaldrik R. Postema[†,‡] and Paul Smith[*,‡,§]

Materials Department and Department of Chemical & Nuclear Engineering, University of California at Santa Barbara, Santa Barbara, California 93106

Received September 25, 1989; Revised Manuscript Received January 29, 1990

ABSTRACT: The stiffness of oriented, flexible-chain polymers is discussed. This paper elaborates on a previously introduced theory for the development of the axial Young's modulus with the draw ratio of flexible macromolecules. Here, the model is applied to uniaxially oriented poly(ethylene terephthalate), poly(oxymethylene), isotactic polypropylene, and poly(*p*-xylylene). Special attention is devoted to the prediction of the limits, set by the molecular weight, to the maximum Young's modulus that can be achieved through tensile drawing.

Introduction

In a previous paper[1] a simple theory was presented for the development of the axial Young's modulus with a draw ratio of flexible-chain molecules. The model is based on the assumption that orientational drawing of flexible polymers proceeds in an affine fashion; its applicability is therefore limited to experimental conditions favoring affine deformation, such as relatively low drawing temperatures. In the model, the partially oriented polymer is considered to be comprised of only two types of elastic elements; "helix" elements, which are perfectly oriented in the direction of the draw, and "coil" elements, which are unoriented. Tensile drawing is understood to increase the fraction, f_h, of helix elements at the expense of the fraction of coil elements, $1 - f_h$. The two elements are characterized by their respective moduli: E_h, the theoretical axial chain modulus, and E_u, the modulus of the unoriented material in which, strictly speaking, $f_h = 0$. The rationale for this simple two-state approach, which was previously employed by Hermans[2] and Fraser,[3] finds its origin in the recognition that the stiffness of most oriented polymers is extremely anisotropic and that the off-axis modulus is essentially independent of the test direction over a wide range of angles (Ward[4] and Bastiaansen et al.[5]).

Following Ward et al.,[6] the model assumes a uniform stress distribution in the helix and coil elements. On the basis of these assumptions, the Young's modulus of a flexible polymer that is drawn to a draw ratio, λ, is given[1] by the equation

$$E = \left(E_u^{-1} - \left[\frac{3\lambda^3}{2(\lambda^3 - 1)} [1 - (\lambda^3 - 1)^{-1/2} \tan^{-1} \{(\lambda^3 - 1)^{1/2}\}] - \frac{1}{2} \right] (E_u^{-1} - E_h^{-1}) \right)^{-1} \quad (1)$$

which for $\lambda \geq 5$ to good approximation reduces to

$$E = \left[E_h^{-1} + (E_u^{-1} - E_h^{-1}) \left(\frac{3\pi}{4}\right) \lambda^{-3/2} \right]^{-1} \quad (2)$$

It is of interest to note that a plot of E^{-1} vs $\lambda^{-3/2}$, at sufficiently high values of λ, is predicted to yield a straight line with slope $(E_u^{-1} - E_h^{-1})(3\pi/4)$ and an intercept at $\lambda^{-3/2} = 0$ of E_h^{-1} (the reciprocal theoretical modulus). This implies that the model is particularly well-suited to predict theoretical axial moduli of flexible-chain polymers.

Equations 1 and 2 do not contain any molecular weight dependent variables or parameters. Thus the model predicts, in agreement with numerous experimental observations, that the Young's modulus depends uniquely on the absolute draw ratio, provided that deformation proceeded in a (near) affine mode. The molecular weight, or rather chain length, does set an upper limit, however, to the average maximum ratio, $\lambda_{max,net}$, to which a molecular network can be elongated.[7,8] The latter quantity to a good approximation (for values of $\lambda > 2$) is given by

$$\lambda_{max,net} = (3)^{1/2}(l_p/l)(n/C_\infty)^{1/2} \quad (3)$$

Here n is the number of chain segments, having a length l and a projected length l_p in the chain direction and C_∞ is the characteristic ratio.[7,9] (The prefactor $(3)^{1/2}$, which was not considered in ref 1, stems from network considerations.[8]) This maximum draw ratio directly trans-

† Present address: ICI Europa Ltd., Everslaan 45, B-3078 Kortenberg, Belgium.
‡ Materials Department.
§ Department of Chemical & Nuclear Engineering.

0024-9297/90/2223-3296$02.50/0